Arab. J. Math. (2015) 4:185–197
DOI 10.1007/s40065-015-0131-z

Arabian Journal of Mathematics

Rajeswari Seshadri · **Shankar Rao Munjam**

Heat transfer near the stagnation point of an unsteady three-dimensional flow

Received: 31 December 2014 / Accepted: 28 May 2015 / Published online: 11 June 2015

Abstract In this paper, the unsteady laminar three-dimensional flow of an incompressible viscous fluid in the neighbourhood of a stagnation point is studied. The magnetic field is applied normal to the surface and the effects of viscous dissipation and Ohmic heating are taken into account. The unsteadiness in the flow is caused by the external free stream varying arbitrarily with time. The governing equations are solved both analytically and numerically. An approximate analytical solution has been obtained for flow and heat transfer in the form of series solution using Homotopy Analysis Method while the numerical solutions are computed using the Runge–Kutta–Fehlberg Method with a shooting technique. The influence of various parameters such as the viscous dissipation, unsteadiness, ratio of the velocity gradient and magnetic field effects on flow and heat transfer parameters are studied. A detailed error analysis is done to compute the averaged square residual errors for velocity and temperature. The optimal values of the convergence control parameter are computed for the flow which is used for obtaining all the other results presented.

Mathematics Subject Classification 74G10 · 76N20 · 76W05 · 76D05

الملخص

في هذه الورقة، ندرس التدفق الرقيقي ثلاثي الأبعاد غير المستقر لمائع لزج غير قابل للضغط في جوار نقطة ركود. يؤثر الحقل المغناطيسي بشكل عمودي على السطح ويتم أخذ تأثيرات التبديد اللزج والتسخين الأومي بعين الاعتبار. المتسبب في عدم الاستقرار هو تيار حر يتغير بشكل اعتباطي مع مرور الزمن. يتم حل المعادلات الحاكمة تحليلياً وعددياً. تم الحصول على حل تحليلي تقريبي للتدفق وانتقال الحرارة على شكل حل متسلسلة باستخدام طريقة التحليل التشويهي (HAM) بينما يتم احتساب الحلول العددية باستخدام طريقة رنجا – فلبرغ مع تقنية الرماية (RKFM). تتم دراسة تأثير المعلمات المختلفة مثل التبديد اللزج، وعدم الاستقرار، ونسبة التدرج والحقل المغناطيسي على التدفق ومعلمات انتقال الحرارة. يجرى أيضا تحليل مفصّل للخطأ لحساب الأخطاء المتبقية المربعة المُوَسَّطة للسرعة ودرجة الحرارة. يتم احتساب القيم المُثْلى لمعلم سيطرة التقارب للتدفق الذي يستخدم للحصول على جميع النتائج التي يتم تقديمها.

1 Introduction

The study of laminar boundary layers to variations in the external free stream with time has many practical applications in flow over helicopters; missile aerodynamics; turbo-machines and in flutter phenomena involving

R. Seshadri (✉) · S. R. Munjam
Department of Mathematics, Ramanujan School of Mathematical Sciences, Pondicherry University, Pondicherry 605014, India
E-mail: oviaraji@yahoo.com

S. R. Munjam
E-mail: munjam.shankarrao11@gmail.com

wings. The unsteadiness increases the complexities of the problem because the dimension of the problem is increased. During recent years, the subject of unsteady boundary layer studies near stagnation region has received considerable attention.

The three-dimensional laminar incompressible boundary-layer flow in the neighbourhood of the nodal point region (i.e., $0 \leq c \leq 1$) was first studied by Howarth [1]. The corresponding flow near the saddle point region (i.e., $-1 \leq c < 0$) was considered by Davey [2] where he has observed the appreciable changes in the similarity solution of boundary layer equations compared to the solution near the nodal point region. The heat transfer in the three-dimensional stagnation flow at nodal point region has been analysed by Cheng et al. [3] and a self-similar solution has been obtained.

The unsteady incompressible flow of a viscous fluid near the stagnation region of a three-dimensional body was investigated by Kumari and Nath [4]. The unsteady heat flux at a general three-dimensional body when the velocity is varying as a linear function of time was considered by Teipel [5]. A stagnation point solution near nodal and saddle point regions of an incompressible micro polar fluid was studied by Guram et al. [6]. The effect of the magnetic field on the stagnation point flow and heat transfer of a viscous fluid was studied by Kumari et al. [7]. The unsteady stagnation point flow of a stretching surface in a three-dimensional flow was studied by Rajeswari et al. [8]. Various aspects of this problem were studied by the authors [9,10]. The unsteady laminar MHD flow of a viscous fluid with variation of Ohmic heating and viscous dissipation was studied by Osalusi et al. [11], as well as [12,13].

The importance of studying the unsteady boundary layer flow near stagnation region is that the heat transfer is maximum near the stagnation point. When the free stream velocity varies arbitrarily with time, unsteadiness is caused in the flow field. This unsteadiness influences the flow and heat transfer to a great extent. Most of the studies cited above present the numerical solutions of flow and heat transfer near the stagnation point. Our aim is to obtain an approximate analytical solution for the flow velocity and the temperature in the form of a power series solution. Since the approximate analytical solution for the three-dimensional stagnation point boundary layer flow has not been studied, we obtain the same using Homotopy Analysis Method (HAM). Since this method is described in detail in [14,15], it is not explained here for the sake of brevity.

Generally, HAM solutions are always represented as a power series form in which the coefficients contain the study parameters. In our analysis the various study parameters considered are magnetic field strength (M); unsteadiness in the flow (λ); Prandtl number (Pr); the ratio of the velocity gradient c and the viscous dissipation parameters α and β. We have also computed the numerical solutions for our governing equations using the Runge–Kutta–Fehlberg (RKF) method with shooting technique.

2 Problem formulation and governing equation

We consider the unsteady incompressible viscous flow of an electrically conducting fluid in the neighbourhood of a stagnation point of a three-dimensional surface. Let us consider the orthogonal set of coordinates (x, y, z) with the origin "O" at the forward stagnation region, with x and y coordinates along the body surface and z is the coordinate perpendicular to the body surface at origin as shown in Fig. 1. The unsteadiness in the flow field is imparted by the free stream varying arbitrarily with time.

Uniform magnetic field of strength B is applied normal to the surface in the positive z direction. Since the magnetic Reynolds number is considered to be small, the induced magnetic field can be neglected. The effects of viscous dissipation and Ohmic heating are taken into account. The Navier–Stokes equations governing the three dimensional flow and heat transfer are given by

$$u_x + v_y + w_z = 0 \tag{1}$$

$$u_t + uu_x + vu_y + wu_z = -\left(p_x - \nu\rho\nabla^2 u + \sigma B^2 u\right)/\rho \tag{2}$$

$$v_t + uv_x + vv_y + wv_z = -\left(p_y - \nu\rho\nabla^2 v + \sigma B^2 v\right)/\rho \tag{3}$$

$$w_t + uw_x + vw_y + ww_z = -\left(p_z - \nu\rho\nabla^2 w\right)/\rho \tag{4}$$

$$\rho C_\rho \left(T_t + uT_x + vT_y + wT_z\right) = \kappa\nabla^2 T + \mu\left(u_z^2 + v_z^2\right) + \sigma B^2\left(u^2 + v^2\right) \tag{5}$$

The initial conditions when $t = 0$ are

$$u = u_i;\ v = v_i;\ w = w_i;\ p = p_i;\ T = T_i \tag{6}$$

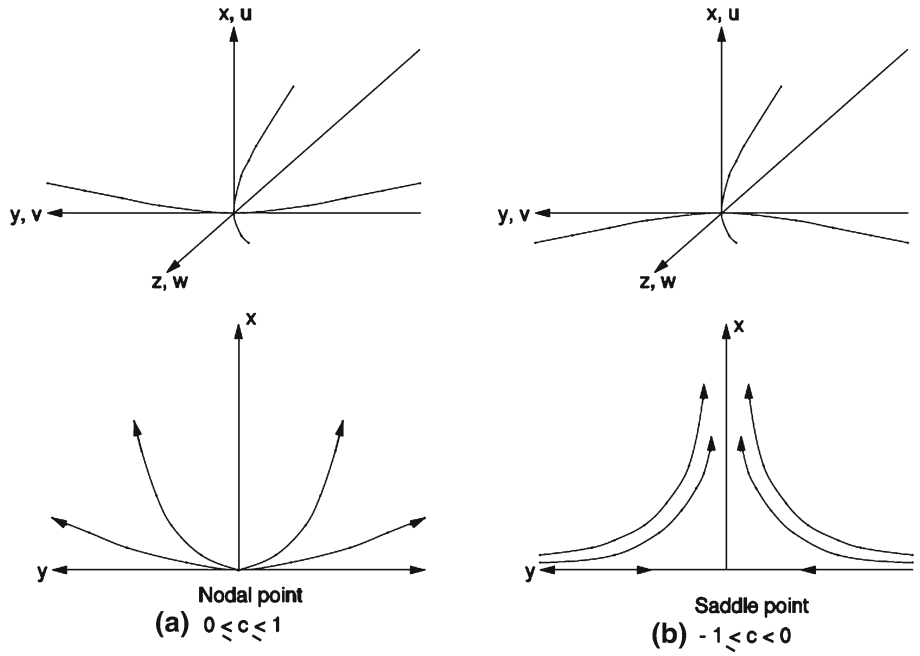

Fig. 1 Coordinate system of velocity components and external streamlines

The boundary conditions are

$$\begin{gathered} u = v = w = 0,\ p = p_0,\ T = T_w \ \text{ at } \ z = 0,\ x \geq 0 \ \text{ and } \ y \geq 0 \\ u \to U,\ v \to V,\ w \to W,\ T \to T_\infty \ \text{ at } \ z \to \infty,\ x \geq 0 \ \text{ and } \ y \geq 0 \\ u = U,\ v = V,\ w = W,\ T = T_\infty \ \text{ at } \ x = 0,\ y \geq 0 \ \text{ and } \ z \geq 0 \\ u = U,\ v = V,\ w = W,\ T = T_\infty \ \text{ at } \ y = 0,\ \ x \geq 0 \ \text{ and } \ z \geq 0. \end{gathered} \tag{7}$$

Here T is the temperature; κ is the thermal conductivity; p is the static pressure; ρ is the density; ν is the kinematic viscosity; C_ρ is the specific heat at a constant pressure; p_0 is the stagnation pressure; B is the magnetic field; U, V and W are the components of velocity in the potential flow; the subscripts t, x, y and z denote the derivatives with respect to t, x, y and z, respectively.

The velocity components in x- and y-directions in the potential flow vary directly as a linear function of distance and inversely as a linear function time.

$$U = (ax)/(1 - \lambda t), \quad V = (by)/(1 - \lambda t) \ \text{ where } \ \lambda t < 1 \tag{8}$$

The velocity components in z-direction is obtained from Eq. (1) so that the continuity equation is satisfied exactly.

$$W = -az(1 + c)/(1 - \lambda t)$$

The magnetic field B for the unsteady flow and the wall temperature T_w varies as

$$B = B_0/\sqrt{(1 - \lambda t)} \quad \text{and} \quad (T_w - T_\infty) = (T_{w0} - T_\infty)/(1 - \lambda t)^2, \tag{9}$$

where T_{w_0} is the value of T_w when $t = 0$.

The expression of pressure p can be obtained from Bernoulli equation as

$$p_0 - p = (\rho a^2)/2(1 - \lambda t)^2 \left[(1 + \lambda + M)\, x^2 + c\,(c + \lambda + M)\, y^2 + (1 + c)\,(1 + c - \lambda)\, z^2\right] \tag{10}$$

Since the governing equations are a system of partial differential Eqs. (1–5) with four independent variables $(x,\ y,\ z,\ t)$, we apply a suitable similarity transformation by which the partial differential equations can be converted into a system of nonlinear ordinary differential equations.

The similarity transformations are

$$\eta = (a/\nu)^{1/2}(1-\lambda t)^{-1/2} z, \quad u = ax(1-\lambda t)^{-1} f'(\eta), \quad v = by(1-\lambda t)^{-1} g'(\eta) \tag{11a}$$

$$\text{and } w = -(a\nu)^{1/2}(1-\lambda t)^{-1/2}[f(\eta) + cg(\eta)], \tag{11b}$$

$$T - T_\infty = (T_w - T_\infty)[s(\eta) + (x/L)^2 \Phi(\eta) + (y/L)^2 \theta(\eta)] = (T_w - T_\infty) s(\eta) \tag{11c}$$

$$p_0 - p = (\rho a^2)/2(1-\lambda t)^2 \left[(1+\lambda+M)\, x^2 + c\,(c+\lambda+M)\, y^2 + (2\nu/a)\,(1-\lambda t)\, P(\eta)\right], \tag{11d}$$

where $M = \sigma B_0^2/\rho a$. Here s, Φ and θ used in temperature represent the dimensionless temperatures without viscous dissipation, with viscous dissipation and with Ohmic heating, respectively.

Substituting Eqs. (11a–11d) into Eqs. (1–5), we find that Eq. (1) is identically satisfied and Eqs. (2–5) reduce to a system of coupled non-linear ordinary differential equations given by

$$f''' + (f+cg) f'' + 1 - (f')^2 + M(1-f') + \lambda(1 - f' - \eta f''/2) = 0 \tag{12}$$

$$g''' + (f+cg) g'' + c\left(1 - (g')^2\right) + M(1-g') + \lambda(1 - g' - \eta g''/2) = 0 \tag{13}$$

$$\mathrm{Pr}^{-1} s'' + (f+cg) s' - 2^{-1}\eta s' - 2\lambda s = 0 \tag{14}$$

$$\mathrm{Pr}^{-1}\Phi'' + (f+cg)\Phi' - 2f'\Phi - 2\lambda\Phi - 2^{-1}\eta\lambda\Phi' + \alpha\left[(f'')^2 + M(f')^2\right] = 0 \tag{15}$$

$$\mathrm{Pr}^{-1}\theta'' + (f+cg)\theta' - 2cg'\theta - 2\lambda\theta - 2^{-1}\eta\lambda\theta' + \beta\left[(g'')^2 + M(g')^2\right] = 0 \tag{16}$$

$$P = 2^{-1}(f+cg)^2 - (\lambda/2)\,\eta\,(f+cg). \tag{17}$$

Equation (17) has been written after integration satisfying the condition on pressure.

The boundary conditions are

$$f(0) = 0, \quad f'(0) = 0, \quad f'(\infty) = 1; \quad g(0) = 0, \quad g'(0) = 0, \quad g'(\infty) = 1$$

$$s(0) = 1, \quad s(\infty) = 0; \quad \Phi(0) = 0, \quad \Phi(\infty) = 0; \quad \theta(0) = 0, \quad \theta(\infty) = 0. \tag{18}$$

Here f' and g' are the dimensionless velocity components in x- and y-directions, respectively; λ is the unsteadiness parameter; η is the similarity variable; M is the magnetic parameter; Pr is the Prandtl number; a and b are the velocity gradient along x- and y-directions in the potential flow; $c = b/a$ is ratio of the velocity gradient; α and β are the viscous dissipation parameters; $L = (\nu/a)^{1/2}$ is the characteristic length and prime denotes derivative with respect to η.

Equations (12–16) with $\lambda = 0$ (steady-state case) and without Ohmic heating (i.e., magnetic parameter $M = 0$) are the same as those of [1] for the flow in the nodal point region ($0 \le c \le 1$) and to those of [2] in the saddle point region ($-1 \le c < 0$). Further may be noted that Eqs. (12–16) without the last term in (14) for $M = 0$ are same to those of [5].

The heat transfer coefficient in terms of Nusselt number and local Skin friction coefficients in x and y directions are expressed as

$$C_{fx} = 2\mu(\partial u/\partial z)_{z=0}/\rho U^2 = 2(Re)^{-1/2} f''(0)$$

$$C_{fy} = 2\mu(\partial v/\partial z)_{z=0}/\rho U^2 = 2(V/U)(Re)^{-1/2} g''(0)$$

$$Nu_x = -x(\partial T/\partial z)_{z=0}/(T_w - T_\infty) = -(Re_x)^{1/2}\left[s'(0) + (x/L)^2\Phi'(0) + (y/L)^2\theta'(0)\right] = -(Re_x)^{1/2} s'(0)$$

where $Re_x = Ux/\nu$.

3 HAM solution

The main features of the HAM procedure are selecting suitable initial profiles satisfying the boundary conditions of the problem concerned; choosing an appropriate linear operator so that its solutions are simpler to evaluate analytically. The initial profiles that satisfy the initial and boundary conditions of the flow are

$$f_0(\eta) = \eta + 1 - e^{-\eta}, \quad g_0(\eta) = \eta + 1 - e^{-\eta}, s_0(\eta) = 1 - e^{-\eta}, \quad \Phi_0(\eta) = \eta e^{-\eta}, \quad \theta_0(\eta) = \eta e^{-\eta}. \tag{19}$$

$$L_f = \frac{\mathrm{d}^3 f}{\mathrm{d}\eta^3} - \frac{\mathrm{d}f}{\mathrm{d}\eta}, \; L_g = \frac{\mathrm{d}^3 g}{\mathrm{d}\eta^3} - \frac{\mathrm{d}g}{\mathrm{d}\eta}, \quad L_s = \frac{\mathrm{d}^2 s}{\mathrm{d}\eta^2} - s, \quad L_\Phi = \frac{\mathrm{d}^2 \Phi}{\mathrm{d}\eta^2} - \Phi, \quad L_\theta = \frac{\mathrm{d}^2 \theta}{\mathrm{d}\eta^2} - \theta, \tag{20}$$

The Linear Operator chosen for this set of equations are

$$L_f\left[C_1 + C_2 e^{\eta} + C_3 e^{-\eta}\right] = 0, L_g\left[C_4 + C_5 e^{\eta} + C_6 e^{-\eta}\right] = 0, \quad L_s\left[C_7 e^{\eta} + C_8 e^{-\eta}\right] = 0,$$
$$L_\Phi\left[C_9 e^{\eta} + C_{10} e^{-\eta}\right] = 0, \quad L_\theta\left[C_{11} e^{\eta} + C_{12} e^{-\eta}\right] = 0, \tag{21}$$

in which C_i are the arbitrary constants.

The nonlinear operator is directly written from the governing equation of the problem. We choose the set of base functions and initial guesses, auxiliary linear operators as follows:

$$\left\{\left(\eta^k e^{-n\eta}\right), k \geq 0, n \geq 0\right\}$$

Then, we can write

$$X(\eta) = A^0_{0,0} + \sum_{n=0}^{\infty}\sum_{k=0}^{\infty}\left[A^k_{\ell,n}\eta^k e^{-n\eta}\right], \tag{22}$$

where X here denotes our study variables and $X = f,\ g,\ s,\ \Phi,\ \theta$ and $A^k_{\ell,n}$ are the coefficients.

3.1 Zeroth and higher-order deformation problems

To obtain the HAM solution for the governing Eqs. (12–16), let $\tau \in [0, 1]$ be an embedding parameter and c_f, c_g and c_s, c_Φ, c_θ be the basic convergence control parameters. Then the zeroth order deformation equation and the non-linear operators take the following form:

$$(1-\tau)L_X[X(\eta,\tau) - X_0(\eta)] = \tau c_X \mathcal{N}_X[X(\eta,\tau)], \tag{23}$$

where $X = f,\ g,\ s,\ \Phi$ and θ; $X_0 = f_0,\ g_0,\ s_0,\ \Phi_0$ and θ_0.

$$\mathcal{N}_f[f(\eta,\tau)] = \frac{\partial^3 f(\eta,\tau)}{\partial\eta^3} + (f(\eta,\tau) + cg(\eta,\tau))\left(\frac{\partial^2 f(\eta,\tau)}{\partial\eta^2}\right) + \left(1 - \left(\frac{\partial f(\eta,\tau)}{\partial\eta}\right)^2\right)$$
$$+M\left(1 - \left(\frac{\partial f(\eta,\tau)}{\partial\eta}\right)\right) + \lambda\left(1 - \left(\frac{\partial f(\eta,\tau)}{\partial\eta}\right) - \left(\frac{\eta}{2}\right)\left(\frac{\partial^2 f(\eta,\tau)}{\partial\eta^2}\right)\right) \tag{24}$$

$$\mathcal{N}_g[g(\eta,\tau), f(\eta,\tau)] = \frac{\partial^3 g(\eta,\tau)}{\partial\eta^3} + (f(\eta,\tau) + cg(\eta,\tau))\left(\frac{\partial^2 g(\eta,\tau)}{\partial\eta^2}\right) + c\left(1 - \left(\frac{\partial g(\eta,\tau)}{\partial\eta}\right)^2\right)$$
$$+M\left(1 - \left(\frac{\partial g(\eta,\tau)}{\partial\eta}\right)\right) + \lambda\left(1 - \left(\frac{\partial g(\eta,\tau)}{\partial\eta}\right) - \left(\frac{\eta}{2}\right)\left(\frac{\partial^2 g(\eta,\tau)}{\partial\eta^2}\right)\right) \tag{25}$$

$$\mathcal{N}_s[s(\eta,\tau), g(\eta,\tau), f(\eta,\tau)] = \mathrm{Pr}^{-1}\left(\frac{\partial^2 s(\eta,\tau)}{\partial\eta^2}\right) + (f(\eta,\tau) + cg(\eta,\tau))\left(\frac{\partial s(\eta,\tau)}{\partial\eta}\right) - \left(\frac{\eta}{2}\right)\left(\frac{\partial s(\eta,\tau)}{\partial\eta}\right)$$
$$-2\lambda s(\eta,\tau) \tag{26}$$

$$\mathcal{N}_\Phi[\Phi(\eta,\tau), g(\eta,\tau), f(\eta,\tau)] = \mathrm{Pr}^{-1}\left(\frac{\partial^2\Phi(\eta,\tau)}{\partial\eta^2}\right) + (f(\eta,\tau) + cg(\eta,\tau))\left(\frac{\partial\Phi(\eta,\tau)}{\partial\eta}\right) - 2\left(\frac{\partial f(\eta,\tau)}{\partial\eta}\right)\Phi(\eta,\tau) \tag{27}$$

$$-\lambda\Phi(\eta,\tau) - \left(\frac{\eta}{2}\right)\lambda\Phi(\eta,\tau) + \alpha\left[\left(\frac{\partial^2 f(\eta,\tau)}{\partial\eta^2}\right)^2 + M\left(\frac{\partial f(\eta,\tau)}{\partial\eta}\right)^2\right] \tag{28}$$

$$\mathcal{N}_\theta[\theta(\eta,\tau), g(\eta,\tau), f(\eta,\tau)] = \mathrm{Pr}^{-1}\left(\frac{\partial^2\theta(\eta,\tau)}{\partial\eta^2}\right) + (f(\eta,\tau) + cg(\eta,\tau))\left(\frac{\partial\theta(\eta,\tau)}{\partial\eta}\right) \tag{29}$$

$$-2c\left(\frac{\partial g(\eta,\tau)}{\partial\eta}\right)\theta(\eta,\tau) - 2\lambda\theta(\eta,\tau) - \left(\frac{\eta}{2}\right)\lambda\theta(\eta,\tau) + \beta\left[\left(\frac{\partial^2 g(\eta,\tau)}{\partial\eta^2}\right)^2 + M\left(\frac{\partial g(\eta,\tau)}{\partial\eta}\right)^2\right] \tag{30}$$

with appropriate boundary conditions from Eq. (18) we have

$$f(\eta;\tau)|_{\eta=0} = g(\eta;\tau)|_{\eta=0} = 0, \quad \left.\frac{\partial f(\eta;\tau)}{\partial\eta}\right|_{\eta=0} = \left.\frac{\partial g(\eta;\tau)}{\partial\eta}\right|_{\eta=0} = 0, \quad \left.\frac{\partial f(\eta;\tau)}{\partial\eta}\right|_{\eta=\infty} = \left.\frac{\partial g(\eta;\tau)}{\partial\eta}\right|_{\eta=\infty} = 1,$$

$$s(\eta;\tau)|_{\eta=0} = 1,\ \Phi(\eta;\tau)|_{\eta=0} = \theta(\eta;\tau)|_{\eta=0} = 0, \quad s(\eta;\tau)|_{\eta=\infty} = \Phi(\eta;\tau)|_{\eta=\infty} = \theta(\eta;\tau)|_{\eta=\infty} = 0, \tag{31}$$

For ℓth-order deformation equations, we first differentiate Eq. (23) ℓ- times with respect to τ, dividing them by $\ell!$ and then set $\tau = 0$. Following this we have

$$L_X[X_\ell(\eta) - \Omega_\ell X_{\ell-1}(\eta)] = c_X\mathcal{R}_\ell^X(\eta) \tag{32}$$

with boundary conditions

$$\begin{aligned} &f_\ell(0) = g_\ell(0) = 0,\ f'_\ell(0) = g'_\ell(0) = 0,\ f'_\ell(\infty) = g'_\ell(\infty) = 1 \\ &s_\ell(0) = 1,\ \Phi_\ell(0) = \theta_\ell(0) = 0,\ s_\ell(\infty) = \Phi_\ell(\infty) = \theta_\ell(\infty) = 0 \end{aligned} \tag{33}$$

where the remainder term $\mathcal{R}_\ell^X(\eta)$ are expanded and rewritten from the governing Eqs. (12–16) as follows:

$$\mathcal{R}_\ell^f(\eta) = f'''_{\ell-1}(\eta) + \sum_{j=0}^{\ell-1}\left[f_{\ell-1-j}f''_j - f'_{\ell-1-j}f'_j\right] + c\sum_{j=0}^{\ell-1}\left[g_{\ell-1-j}f''_j\right] + \left(1 + M\left[1 - f'_{\ell-1}(\eta)\right]\right) + \lambda\left[1 - f'_{\ell-1}(\eta) - \left(\frac{\eta}{2}\right)f''_{\ell-1}(\eta)\right] \tag{34}$$

$$\mathcal{R}_\ell^g(\eta) = g'''_{\ell-1}(\eta) + \sum_{j=0}^{\ell-1}[f_{\ell-1-j}g''_j] + c\sum_{j=0}^{\ell-1}\left[g_{\ell-1-j}g''_j - g'_{\ell-1-j}g'_j\right] + \left(c + M\left[1 - g'_{\ell-1}(\eta)\right]\right) + \lambda\left[1 - g'_{\ell-1}(\eta) - \left(\frac{\eta}{2}\right)g''_{\ell-1}(\eta)\right] \tag{35}$$

$$\mathcal{R}_\ell^s(\eta) = \mathrm{Pr}^{-1}s''_{\ell-1}(\eta) + \sum_{j=0}^{\ell-1}[f_{\ell-1-j}\ s'_j(\eta)] + c\sum_{j=0}^{\ell-1}[g_{\ell-1-j}\ s'_j(\eta)] - \left(\frac{\eta}{2}\right)s'_{\ell-1}(\eta) - 2\lambda s_{\ell-1}(\eta) \tag{36}$$

$$\mathcal{R}_\ell^\Phi(\eta) = \mathrm{Pr}^{-1}\Phi''_{\ell-1}(\eta) + \sum_{j=0}^{\ell-1}[f_{\ell-1-j}\ \Phi'_j(\eta)] + c\sum_{j=0}^{\ell-1}[g_{\ell-1-j}\ \Phi'_j(\eta)] - 2\sum_{j=0}^{\ell-1}[f'_{\ell-1-j}\ \Phi_j(\eta)] - \lambda\Phi_{\ell-1}(\eta) - \left(\frac{\lambda\eta}{2}\right)\Phi_{\ell-1}(\eta) + \alpha\left[\sum_{j=0}^{\ell-1}[f''_{\ell-1-j}f''_j + Mf'_{\ell-1-j}f'_j]\right] \tag{37}$$

$$\mathcal{R}_\ell^\theta(\eta) = \mathrm{Pr}^{-1}\theta''_{\ell-1}(\eta) + \sum_{j=0}^{\ell-1}[f_{\ell-1-j}\ \theta'_j(\eta)] + c\sum_{j=0}^{\ell-1}[g_{\ell-1-j}\ \theta'_j(\eta)] - 2c\sum_{j=0}^{\ell-1}[g'_{\ell-1-j}\ \theta_j(\eta)]$$
$$-2\lambda\theta_{\ell-1}(\eta) - \left(\frac{\lambda\eta}{2}\right)\theta_{\ell-1}(\eta) + \beta\left[\sum_{j=0}^{\ell-1}[g''_{\ell-1-j}g''_j + Mg'_{\ell-1-j}g'_j]\right], \tag{38}$$

where Ω_ℓ defines as

$$\Omega_\ell = \begin{cases} 0 & \text{if } \ell \le 1 \\ 1 & \text{if } \ell > 1. \end{cases} \tag{39}$$

Using Taylor's series, $X(\eta;\tau)$ can be expanded in terms of τ as follows:

$$X(\eta;\tau) = X_0(\eta) + \sum_{\ell=1}^{\infty} X_\ell(\eta)\tau^\ell, \text{ where } X_\ell(\eta) = \frac{1}{\ell!}\frac{\partial^\ell X(\eta;\tau)}{\partial\tau^\ell}\bigg|_{\tau=0}. \tag{40}$$

The auxiliary parameters are selected as $\tau = 0$ and $\tau = 1$ from Eq. (23), one may write

$$X(\eta;0) = X_0(\eta), \quad X(\eta;1) = X(\eta). \tag{41}$$

Thus as τ increases from 0 to 1 and $X(\eta;\tau)$ varies from the initial guess $X_0(\eta)$ to the solution $X(\eta)$ of the governing equations respectively. The auxiliary parameters are selected so that the series solutions converge for $\tau = 1$ and the particular solution is

$$X(\eta) = X_0(\eta) + \sum_{\ell=1}^{\infty} X_\ell(\eta), \tag{42}$$

where $X = f,\ g,\ s,\ \Phi$ and θ; $X_0 = f_0,\ g_0,\ s_0,\ \Phi_0$ and θ_0.

Therefore, we get the general approximate analytical solutions $f_\ell, g_\ell, s_\ell, \Phi_\ell, \theta_\ell$ in terms of special solutions $f_\ell^*, g_\ell^*, s_\ell^*, \Phi_\ell^*, \theta_\ell^*$ as

$$f_\ell(\eta) = f_\ell^*(\eta) + C_1 + C_2e^\eta + C_3e^{-\eta}, \quad g_\ell(\eta) = g_\ell^*(\eta) + C_4 + C_5e^\eta + C_6e^{-\eta} \tag{43}$$

$$s_\ell(\eta) = s_\ell^*(\eta) + C_7e^\eta + C_8e^{-\eta}, \quad \Phi_\ell(\eta) = \Phi_\ell^*(\eta) + C_9e^\eta + C_{10}e^{-\eta}, \quad \theta_\ell(\eta) = \theta_\ell^*(\eta) + C_{11}e^\eta + C_{12}e^{-\eta} \tag{44}$$

We solve Eqs. (43, 44) one after the other in the order $\ell = 1, 2, 3, \ldots$ by means of the symbolic computation software Mathematica. It is shown that the solution for the velocity profile can be expressed as an infinite series of any desired order. It is customary in HAM analysis to draw c_X-curves to identify the interval of optimal convergence control parameter (i.e., c_f and c_g, c_s, c_Φ and c_θ) inside which any suitable values can be chosen. In Fig. 2 it is shown that choosing unique value from the ranges of $c_f \in [-1.6, -0.2]$, $c_g \in [-1.4, -0.1]$ does not affect the values of surface shear stress rates and it is $c_s \in [-1.5, -0.3]$, $c_\Phi \in [-2.1, -0.4]$ and $c_\theta \in [-1.9, -0.5]$ for surface heat transfer rates. The c_X curves have been drawn for 20th order of HAM solution. In all of the figures, we use $\mathrm{Pr} = 0.72$, $\lambda = -1.0$ and $c = -0.5$, $M = 0.5$ and $\alpha = \beta = 0.2$ unless it is mentioned otherwise.

4 Convergence control parameters

In order to choose the optimal values of the convergence control parameters c_X, where $X = f, g, s, \Phi$ and θ, we compute the averaged residual errors suggested by Liao [15].

$$E_X \simeq \frac{1}{\ell}\sum_{j=0}^{i}\left(N\left[\sum_{i=0}^{\ell} X_i(j\Delta x)\right]\right)^2, \tag{45}$$

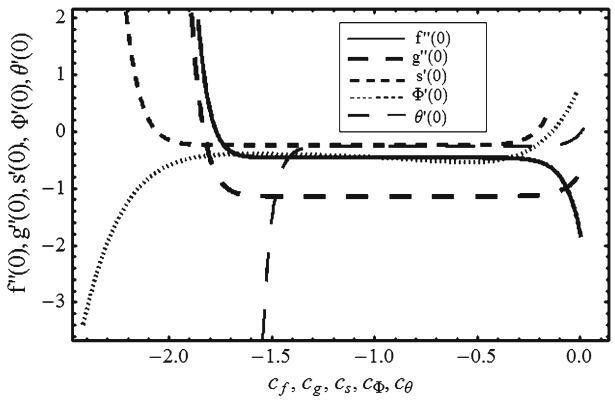

Fig. 2 c_f, c_g, c_s, c_Φ and c_θ-curves

Table 1 The averaged squared residual error E_X with the CPU time at different orders of approximations in HAM analysis

l	CPU minimum of averaged squared residual errors					
	Time (S)	E_f	E_g	E_G	E_Φ	E_θ
2	1.0	2.08642×10^{-2}	2.21558×10^{-3}	6.42071×10^{-3}	1.00611×10^{-6}	1.18235×10^{-4}
4	5.8	1.25201×10^{-4}	1.24501×10^{-5}	2.49866×10^{-5}	3.29999×10^{-7}	2.09782×10^{-7}
6	31.1	2.97143×10^{-7}	3.20537×10^{-8}	1.31442×10^{-8}	1.07162×10^{-9}	5.19336×10^{-10}
8	51.9	4.00527×10^{-9}	4.71582×10^{-10}	2.52719×10^{-11}	2.77611×10^{-11}	4.00001×10^{-13}
10	323.7	9.32769×10^{-12}	5.90002×10^{-13}	9.14281×10^{-14}	6.10022×10^{-13}	3.71102×10^{-14}
12	1281.8	2.62319×10^{-14}	6.00222×10^{-15}	1.71058×10^{-16}	8.29371×10^{-17}	7.33333×10^{-18}
14	1446.1	7.90133×10^{-15}	6.67216×10^{-16}	7.39669×10^{-17}	4.00222×10^{-18}	1.02761×10^{-20}
16	1582.8	2.83001×10^{-17}	5.07803×10^{-19}	1.40772×10^{-20}	7.76201×10^{-21}	6.99728×10^{-21}

where $\Delta x = \frac{10}{\ell}$ and $\ell = 20$. At the ℓ^{th} order, the optimal values of c_X are computed by the minimum of the squared residual E_X of the governing equations, corresponding to

$$\frac{\mathrm{d}E_X}{\mathrm{d}c_X} = 0 \tag{46}$$

The HAM-based *Mathematica package BVPh 2.0*[1] has been used to compute the averaged residual errors of Eqs. (12–16). We use Eq. (45) to find the convergence control parameters and this optimal values obtained are used for the entire computations of flow variables for various values parameters.

The averaged squared residual errors E_X, with the CPU time (S) at different orders of the HAM approximations ℓ are shown in Table 1. The averaged squared residual error decreases rapidly and the optimal values of the convergence control parameters are found to be $c_f = -0.609214$, $c_g = -0.59523$ and $c_s = -0.86576$, $c_\Phi = -1.31155$ and $c_\theta = -0.71554$. Thus the convergence control parameter used in HAM can greatly accelerate the convergence of series solution.

5 Numerical solution

Though several numerical results are available in the literature, to compare our own approximate analytical results for different parametric values, we have performed numerical computation with the simple and still popular technique Runge–Kutta–Fehlberg Method with a shooting technique(RKFM). The numerical solution of the governing Eqs. (12–16) subject to the boundary conditions Eq. (18) have been obtained using the RKFM method. It was necessary to adopt a shooting technique to get the missing slopes $f''(0)$, $g''(0)$ and $-s'(0)$, $-\Phi'(0)$, $-\theta'(0)$) for various physical parameters. The numerical results and approximate analytical results agree very well in all the calculations, some of which are shown in the tables and figures.

[1] Refer. http://numericaltank.sjtu.edu.cn/BVPh.htm.

Table 2 Comparison of skin friction results for steady case ($f''(0)$, $g''(0)$) when $M = \lambda = 0$ for nodal and saddle point regions

c	$f''(0)$			$g''(0)$		
	Kumari et al. [9]	Present HAM	Present RKFM	Kumari et al. [9]	Present HAM	Present RKFM
0.00	1.2268	1.2268084	1.2268084	0.5848	0.5848333	0.5848333
0.25	1.2453	1.2453641	1.2453641	0.8378	0.8378750	0.8378750
0.50	1.2654	1.2654008	1.2654008	1.0142	1.0142396	1.0142396
0.75	1.2892	1.2892765	1.2892765	1.1723	1.1723170	1.1723170
1.00	1.3153	1.3153407	1.3153407	1.3153	1.3153347	1.3153347
−0.2	1.2256	1.2256840	1.2256840	0.3350	0.3350904	0.3350904
−0.4	1.2262	1.2262611	1.2262611	0.0459	0.0459610	0.0459610
−0.6	1.2361	1.2361333	1.2361333	−0.2664	−0.2666421	−0.2666421
−0.8	1.2519	1.2519924	1.2519924	−0.5485	−0.5485740	−0.5485740
−1.0	1.2732	1.2732043	1.2732043	−0.8110	−0.8110879	−0.8110879

Table 3 Comparison of heat transfer rates ($-s'(0)$) for different Pr, when $M = \lambda = 0$ for nodal and saddle point regions

$-s'(0)$						
c	Kumari et al. [9]		Present HAM		Present RKFM	
	Pr = 0.7	Pr = 10.0	Pr = 0.7	Pr = 10.0	Pr = 0.7	Pr = 10.0
0.00	0.4957	1.3386	0.4959980	1.3387713	0.4959980	1.3387713
0.25	0.5358	1.4265	0.5369627	1.4262420	0.5369627	1.4262420
0.50	0.5798	1.5311	0.5784300	1.5320669	0.5784300	1.5320669
0.75	0.6233	1.6419	0.6235361	1.6438587	0.6235361	1.6438587
1.00	0.6656	1.7523	0.6659613	1.7526072	0.6659613	1.7526072
−0.10	–	–	0.5463178	1.5901238	0.5463178	1.5901238
−0.25	–	–	0.6109312	1.6432103	0.6109312	1.6432103
−0.50	–	–	0.6961289	1.7074361	0.6961289	1.7074361
−0.75	–	–	0.7233490	1.8498630	0.7233490	1.8498630
−1.00	–	–	0.8073104	1.9103814	0.8073104	1.9103814

6 Results and discussion

We have studied the effect of various physical parameters such as magnetic parameter M, ratio of the velocity gradient c, unsteady parameter λ on velocity and temperature profiles as well as on skin friction coefficients and heat transfer rates. The approximate analytical solutions for the velocity and temperature are obtained in the form of a power series solution using computer Algebra software *Mathematica*. The expressions for f, g, s, Φ and θ are obtained up to 10th degree polynomial. It is to be mentioned here that, though computations could be done easily up to 16th order of deformations equations, to retain the results up to sixth decimal places accuracy we have stopped at the 10th order. Computations have been carried out for several combinations of parameters λ and M, c, Pr, only some representative results are presented here in the form of Tables 1, 2, 3, 4 and Figs. 2, 3, 4, 5, 6, 7, 8, 9.

For the special case of $M = \lambda = 0$ (in the absence of magnetic and unsteady parameter), Table 2 presents the values of skin friction results for steady case ($f''(0)$, $g''(0)$) with that of [9] for nodal and saddle point regions. It was found to be in very good agreement from the 10th order approximation itself. The comparison of heat transfer results for steady case $-s'(0)$ is presented in Table 3. Here, the values of the heat transfer coefficients in terms of local Nusselt number are small for Pr = 0.7 in comparison to the values for Pr = 10.0. This means that the values of the local Nusselt number increase with an increase in Prandtl number.

It is seen from Table 4 that the skin friction and heat transfer rates ($f''(0)$, $-s'(0)$) for various values of c and M are compared in steady case ($\lambda = 0$) with that of [9]. It is found that the values of local skin friction and heat transfer coefficients in terms of local Nusselt number are small for $c = 0$ in comparison to the values for $c = 1.0$. This means that the values of the local Nusselt number increase with an increase in c corresponding with that of magnetic values. The Figs. 3 and 4 show the effect of our study parameters on the velocity, temperature profiles and Figs. 5, 6, 7, 8, 9 show variation of shear stresses and heat transfer rates.

The effect of magnetic parameter M on the velocity profiles $f'(\eta)$ and $g'(\eta)$ in x-and y-directions and temperature profiles $s(\eta)$, $\phi(\eta)$ and $\theta(\eta)$ are plotted in Figs. 3 and 4. It is observed that there is an overshoot in the velocity profiles as magnetic parameter M increases from 0.5 to 4.0. Overshoot in profiles means there is a sudden increase and an immediate decrease in the flow velocity near the surface. This is due to the fact that the imposition of magnetic field creates a drag-like force, called Lorentz force, in the flow field that

Table 4 Comparison of skin friction and heat transfer rates for steady case ($f''(0)$, $-s'(0)$) when Pr = 0.72 at various values of c and M

c	M	$f''(0)$			$-s'(0)$		
		Kumari et al. [9]	Present HAM	Present RKFM	Kumari et al. [9]	Present HAM	Present RKFM
0.0	0.0	1.2268	1.2269340	1.2269340	0.4957	0.4959982	0.4959982
0.0	0.5	1.4132	1.4133836	1.4133836	0.5069	0.5070253	0.5070253
0.0	1.0	1.5795	1.5791185	1.5791185	0.5156	0.5158103	0.5158103
0.0	2.0	1.8664	1.8665012	1.8665012	0.5287	0.5282495	0.5282495
0.0	4.0	2.3397	2.3420600	2.3420600	0.5461	0.5462691	0.5462691
1.0	0.0	1.3153	1.3107777	1.3107777	0.6656	0.6658604	0.6658604
1.0	0.5	1.4827	1.4826013	1.4826013	0.6794	0.6794317	0.6794317
1.0	1.0	1.6403	1.6459755	1.6459755	0.6911	0.6919000	0.6919000
1.0	2.0	1.9176	1.9210201	1.9210201	0.7091	0.7107628	0.7107628
1.0	4.0	2.3796	2.3789651	2.3789651	0.7340	0.7341152	0.7341152

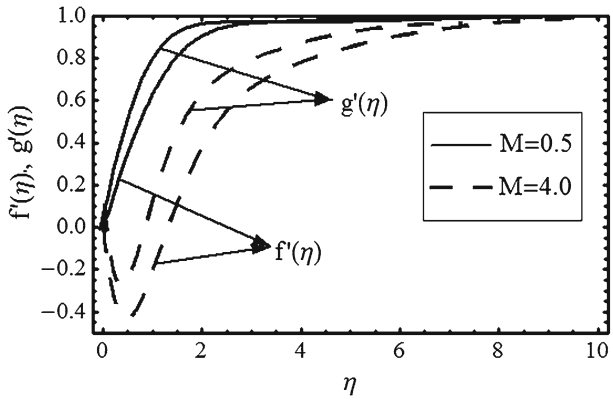

Fig. 3 Effect of the magnetic parameter M on the velocity profiles $f'(\eta)$ and $g'(\eta)$ in x- and y-directions

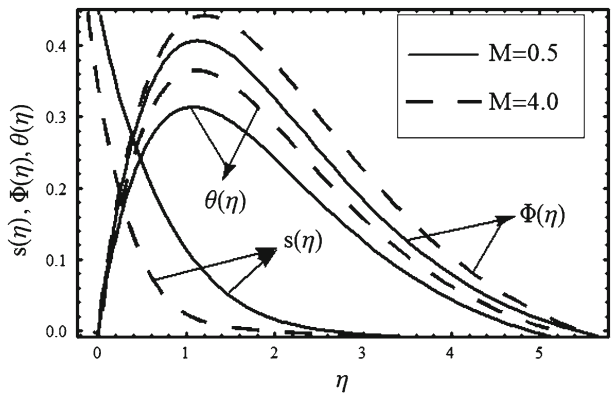

Fig. 4 Effect of the magnetic parameter M on the temperature profiles $s(\eta)$, $\Phi(\eta)$ and $\theta(\eta)$

has the tendency to slow down the flow near the surface, at the same time increasing fluid temperature. As the magnetic field increases, the velocity profile decreases while the temperature profile increases, but the temperature profiles are thinner for higher values of M. The temperature in the absence of viscous dissipation $s(\eta)$ gradually reaches the free stream values, but the behaviour of temperature profiles in the presence of viscous dissipation and Ohmic heating are significantly different in the sense that it increases sharply close to the boundary layer, attains a maximum value and starts decreasing rapidly to attain its free stream values.

The variation of surface shear stress rates in x-and y-directions (i.e., $f''(0)$ and $g''(0)$) and the heat transfer rate ($-s'(0)$, $-\Phi'(0)$ and $-\theta'(0)$) with the unsteady parameter λ for different magnetic parameter M and the different viscous dissipation parameters α, β with ratio of velocity gradient c on the heat transfer rates profile for a fixed value of Pr = 0.7 are presented in Figs. 5, 6, 7, 8, 9. It observed that the decrease in unsteady parameter λ decreases the surface shear stress rates. It is to be noted that the surface shear stress rates ($f''(0)$

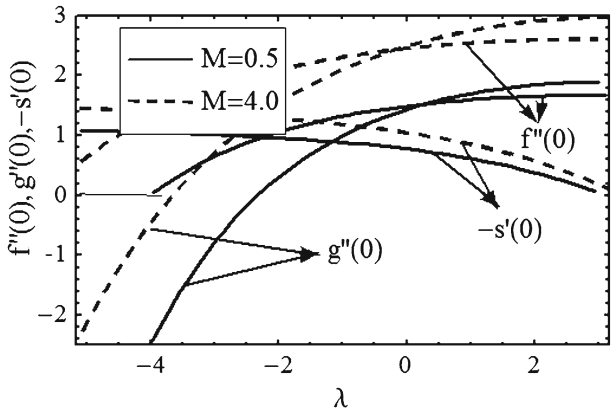

Fig. 5 Effect of the magnetic parameter M on the shear stress rates $f''(0)$ and $g''(0)$ in x- and y-directions and the heat transfer rates $-s'(0)$ at $M = 0.0$, Pr $= 0.7$

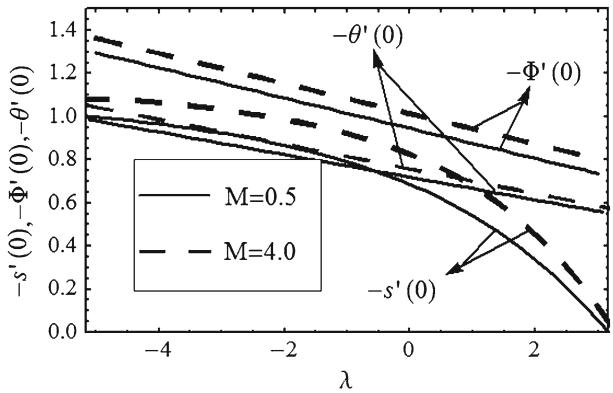

Fig. 6 Effect of the magnetic parameter M on the heat transfer rates

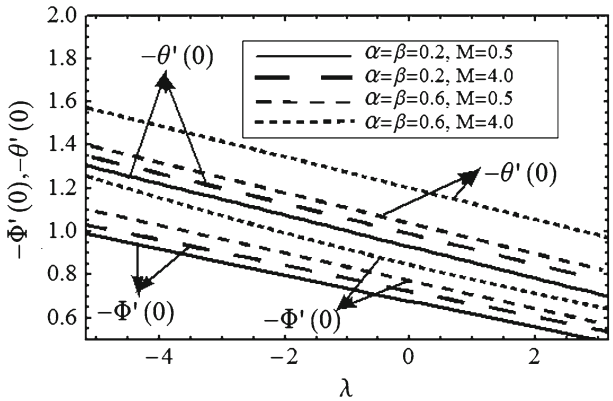

Fig. 7 Effect of the viscous dissipation parameters α, β and magnetic parameter M on the heat transfer rates

and $g''(0)$) in x- and y-directions for every M curve becomes zero for a certain value of unsteady parameter λ. For example, as seen from Fig. 5, $g''(0)$ vanishes at $\lambda = -0.438, -2.189$ for $M = 0.5, 4.0$, respectively. Also, reverse flow occurs for negative values of λ. This means that the decelerating flow behaves like an adverse pressure gradient. Similar trend has been observed by Kumari et al. [9]. The boundary layer thickness increases with decreasing unsteady parameter, which means that the velocity in z-direction increases which in turn increases the heat transfer rate. Hence, as the unsteady parameter λ decreases the heat transfer rate $(-s'(0), -\Phi'(0), -\theta'(0))$ increases as observed from Fig. 6.

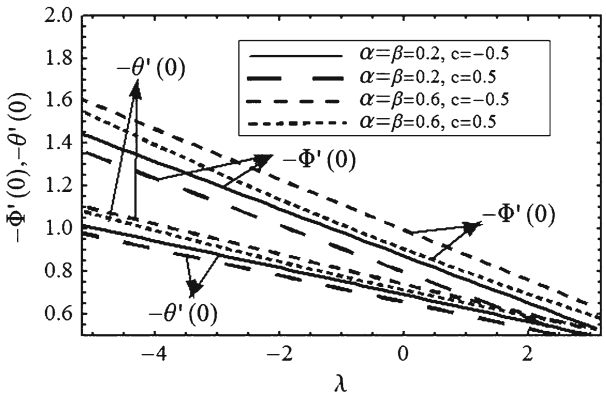

Fig. 8 Effect of the viscous dissipation parameters α, β and ratio of velocity gradient c on the heat transfer rates

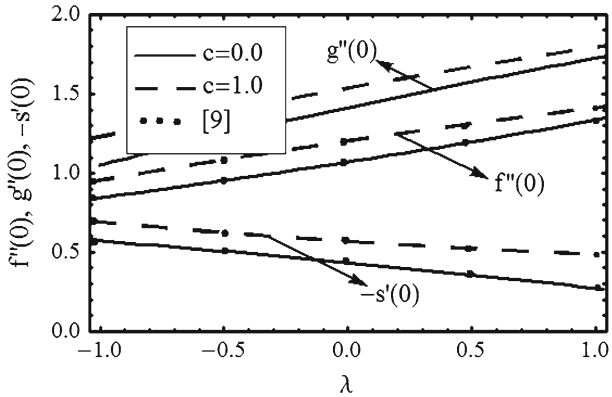

Fig. 9 Comparison of the surface shear stress ($f''(0)$, $g''(0)$), and the heat transfer rates $-s'(0)$ at $M = 0.0$, Pr $= 0.7$ with those of [9]

The effect of the viscous dissipation parameters α, β on the surface heat transfer rate ($-\Phi'(0)$, $-\theta'(0)$), for various values of M, c are presented in Figs. 7 and 8. From Fig. 7, it is observed that, as the unsteady parameter increases, the surface heat transfer ($-\Phi'(0)$ and $-\theta'(0)$) decreases with respect to increase in the magnetic parameter and viscous dissipation parameters. For a given α, β and M, $-\theta'(0)$) values are always higher than $-\Phi'(0)$ values. This is due to the presence of Ohmic heating. Similar to Fig. 7, in Fig. 8, the effect with respect to stretching ratio c is presented. Here surface heat transfers ($-\Phi'(0)$ and $-\theta'(0)$) are found to be higher for saddle point region (c $= -0.5$) compared to its value in the nodal point region ($c = 0.5$).

A comparison result of the shear stress rates (f$''(0)$ and g$''(0)$) and the surface heat transfer rate ($-$s$'(0)$) for two values of c with those of Kumari [9] is shown in Fig. 9. As the unsteadiness in the flow increases the shear stress rates increase where as heat transfer rates decrease.

7 Conclusions

The flow and heat transfer analysis is presented for a three-dimensional viscous fluid flow in the neighborhood of a stagnation point. An approximate analytical expression in the form of a series solution is derived for velocity and temperature using Homotopy Analysis Method. The coefficients of the series solution contain all the study parameters such as c, M and Pr, λ, α, β. The Computer Algebra software Mathematica is used to perform these semi-analytical calculations. The effect of various parameters such as magnetic parameter M, ratio of the velocity gradient parameter c and unsteady parameter λ are analysed on velocity and temperature as well as on surface shear stress rates and heat transfer rates. The accelerating free stream velocity, i.e., $\lambda > 0$ or magnetic parameter M tend to delay or prevent flow reversal. The heat transfer and surface shear stress are found to increase with the increase in the magnetic parameter. Hence it is suggested that by controlling the

magnetic field on suitable strength, one can control the heat transfer rates as well as delay the occurrence of flow reversal near stagnation point region.

Acknowledgments The author Shankar Rao Munjam gratefully acknowledges UGC-Rajiv Gandhi National Fellowship (RGN-SRF), Government of India, for providing financial assistance.

References

1. Howarth. L.: The boundary layer in three dimensional flow. Part II. The flow near a stagnation point. Philos. Mag. **42**, 1433–1440 (1951)
2. Davey, A.: Boundary-layer flow at a saddle point of attachment. J. Fluid. Mech. **10**, 593–610 (1961)
3. Cheng, E.H.W.; Ozisik, M.N.; Williams, J.C.: Nonsteady three-dimensional stagnation-point flow. J. Appl. Mech. **38**, 282–287 (1971)
4. Kumari, M.; Nath, G.: Unsteady laminar compressible boundary-layer flow at a three-dimensional stagnation point. J. Fluid Mech. **87**, 705–717 (1978)
5. Teipel, I.: Heat transfer in unsteady laminar boundary layers at an incompressible three-dimensional stagnation flow. Mech. Res. Comm. **6**, 27–32 (1979)
6. Guram, G.S.; Anwar Kamal, M.: Three-dimensional micropolar flow near saddle and nodal points of attachment. Comput. Math. Appl. **22**, 1–9 (1991)
7. Kumari, M.; Nath, G.: Development of flow and heat transfer of a viscous fluid in the stagnation-point region of a three-dimensional body with a magnetic field. Acta Mech. **135**, 1–12 (1999)
8. Rajeswari, V.; Kumari, M.; Nath, G.: Unsteady stagnation point flow of a three dimensional stretching surface. Acta Mech. **98**, 123–141 (1993)
9. Kumari, M.; Nath, G.: Unsteady flow and heat transfer of a viscous fluid in the stagnation region of a three-dimensional body with a magnetic field. Int. J. Eng. Sci. **40**, 411–432 (2002)
10. Chamkha, A.J.; Ahmed, S.E.: Similarity solution for unsteady MHD flow near a stagnation point of a three-dimensional porous body with heat and mass transfer, heat generation/absorption and chemical reaction. J. Appl. Fluid Mech. **4**, 87–94 (2011)
11. Osalusi, E.; Side, J.; Harris, R.: The effects of Ohmic heating and viscous dissipation on unsteady MHD and slip flow over a porous rotating disk with variable properties in the presence of Hall and ion-slip currents. Int. Commun. Heat Mass Transf. **34**, 1017–1029 (2007)
12. Chauhan, D.S.; Agrawal, R.: Magnetohydrodynamic convection effects with viscous and ohmic dissipation in a vertical channel partially filled by a porous medium. J. Appl. Sci. Eng. **15**, 1–10 (2012)
13. Olanrewaju, P.O.; Bishop, S.A.; Adeeyo, O.A.; Abah, S. A.: Effects of ohmic heating, radiation and viscous dissipation on steady mhd flow near a stagnation point on an isothermal stretching sheet in the presence of heat generation. J. Math. Tech. **2** (2011)
14. Liao, S.J.: An optimal homotopy analysis approach for strongly nonlinear differential equations. Commun. Nonlinear Sci. Numer. Simulat. **15**, 2003–2016 (2010)
15. Liao, S.J.: Homotopy Analysis Method in Nonlinear Differential Equatuions. Springer, New York (2012)